Self-Activation Attenuates the Adverse Effects of Scarce Resources on Genetic Switches

Andras Gyorgy[1]

Abstract—The limited availability of shared cellular resources introduces strong coupling among seemingly unrelated components. Given the fundamental role that multistable switches play in both natural and synthetic genetic systems, here we focus on how the scarcity of resources affects the behavior of these elementary building blocks. In particular, we reveal that while competition for scarce resources pushes the dynamics towards monostability, self-activation attenuates this phenomenon, as well as perturbations from the genetic context of the switch. However, this robustness comes at a price: our analysis uncovers that strong self-activation can lead to tristable dynamics that can surprisingly and misleadingly appear as if the underlying system was monostable, especially when considering cell-to-cell heterogeneity. This paper thus exposes how self-activation and competition for scarce resources establish the stability and robustness properties of genetic switches at both single cell and population levels. Due to their analytic nature, our results provide explicit guidelines for the rational and optimal design of synthetic gene circuits and facilitate the analysis of organizing principles underlying natural systems.

Index Terms—Biological systems, cellular dynamics, modeling, stability of nonlinear systems, systems biology.

I. INTRODUCTION

SYNTHETIC biology seeks to program cellular behavior by combining tools from a diverse set of disciplines, ranging from biotechnology and genetic engineering to control and systems theory [1]. Unfortunately, genetic circuits exhibit context-dependent behavior [2], [3], hindering their rational and computer-aided design [4] due to the absence of reliable and predictive quantitative models. This often leads to iterative and time consuming trial-and-error processes for fine-tuning candidate circuits of even modest complexity [5]. Posing a significant challenge in the progress of synthetic biology, the context-dependent behavior of genetic circuits hence quickly became one of the central research themes at the interface of bioengineering and systems theory.

Due to their shared nature, the scarcity and limited availability of cellular resources fundamentally shapes and intertwines the behavior of genetic circuits [6], [7], [8], [9], [10], often leading to surprising and counter-intuitive phenomena [11]. Characterizing and mitigating these effects represent "system-level" problems [12], requiring a combination of experimental approaches with quantitative tools [13], [14]. Importantly, explicitly accounting for the limited availability of shared cellular resources leads to quantitive models that can accurately predict both *in vitro* and *in vivo* behaviors [9], [15].

Due to the widespread use of multistable switches in both natural and synthetic genetic systems [16], [17], [18], [19], [20], understanding how the scarcity of shared resources shapes their behavior is of paramount importance. Leveraging recent mechanistic models [21], [22], here we uncover how self-activation can attenuate the adverse effects of competition for shared resources.

In particular, in this paper we derive four main results. First, we establish necessary and sufficient conditions for the emergence of mono/bi/tristable dynamics, revealing the role of both self-activation and resource competition. Second, we characterize the robustness of the stable fixed points to noise by combining a potential landscape based approach with the Eyring-Kramers law. Third, we generalize these results to the case when biophysical parameters are random variables to model cell-to-cell heterogeneity ubiquitous to living systems. Finally, we demonstrate that all these results can be generalized to account for competition for scarce resources originating even from the genetic context of the switch. Taken together, these results highlight that while weak self-activation can be beneficial, further increasing it quickly turns disadvantageous. Our analytic results reveal the role that each parameter plays in establishing fundamental properties of multistable genetic switches, thus they provide explicit guidelines for the optimal design of these essential building blocks of both systems and synthetic biology.

This paper is organized as follows. After briefly introducing the mathematical model accounting for both self-activation and the limited availability of shared cellular resources, we reveal how these factors establish the stability and robustness properties of genetic switches, both at the single cell and population levels. Finally, we extend these results to account for competition for scarce resources originating from the genetic context of the switch.

II. MATHEMATICAL MODEL

According to the most widely used model of the toggle switch [16], the dynamics of the proteins y and z inhibiting each other's expression are given by

$$\dot{y} = \frac{\alpha}{1 + z^2} - y, \qquad \dot{z} = \frac{\alpha}{1 + y^2} - z, \qquad (1)$$

where α is the production rate constant. The dynamics in (1) are bistable if $\alpha > 2$ and monostable otherwise [16], [21].

While the above model successfully captures the dynamics of genetic switches that exhibit either monostable or bistable behaviors (Fig. 1), it does not allow for tristability (Fig. 1B), a salient feature of numerous genetic switches with positive
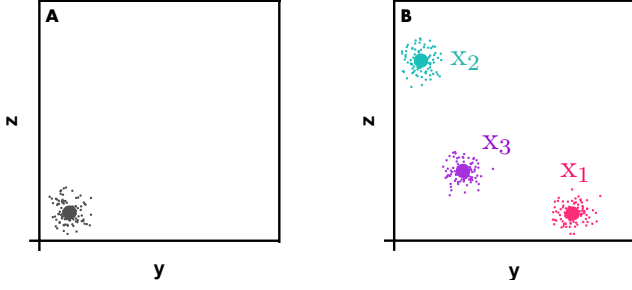
Fig. 1. Depending on the parameter values of (1), the dynamics are either monostable (A) or bistable (B: green and red only). In the case of positive feedback, however, the dynamics in (2) can give rise to a third stable fixed point (B: purple). Stable equilibria of (2) are denoted by circles, whereas small dots show the population level behavior when α and β are drawn from a distribution to model cell-to-cell heterogeneity, as detailed in Section III.C.

feedback via the self-activation of y and z [18], [23], [24]. Additionally, (1) also assumes that cellular resources are abundant, thus it fails to account for coupling due to competition for these shared and scarce resources [8], [9].

To model both these phenomena, introduce the dynamics

$$\dot{y} = \frac{\frac{\alpha}{1+z^2} + \frac{s\alpha y^2}{1+y^2}}{1 + \frac{\beta}{1+y^2} + \frac{\beta}{1+z^2} + \frac{s\beta y^2}{1+y^2} + \frac{s\beta z^2}{1+z^2}} - y,$$
$$\dot{z} = \frac{\frac{\alpha}{1+y^2} + \frac{s\alpha z^2}{1+z^2}}{1 + \frac{\beta}{1+y^2} + \frac{\beta}{1+z^2} + \frac{s\beta y^2}{1+y^2} + \frac{s\beta z^2}{1+z^2}} - z,$$

(2)

where $s\alpha$ denotes the production rate constant due to the positive feedback [18], [23], [24], whereas the lumped constant β decreases the effective production rates, thus it captures loading due to the limited availability of shared resources [8], [9]. As self-activation is considered to be a weak effect, we assume that $0 \leq s \leq 1$. For more details about the lumped parameters α and β, their typical values, and the de-dimensionalization process, see [21], whereas for the effects of parameter asymmetries, see [25].

As competition for shared cellular resources can significantly shape the behavior of genetic circuits [11], here we focus on both the stability of (2) and the robustness of stable fixed points to noise. In particular, we seek to reveal the role that positive feedback (via s) and negative feedback (via β) play in shaping these fundamental properties of multistable genetic switches, both at single cell and population levels, even in the presence of competition originating from the context of the genetic switch. Therefore, in this manuscript we consider three dynamical models: (i) the deterministic model in (2); (ii) its extension for robustness analysis via the overdamped Langevin dynamics [26], [27], [28], [29]; and (iii) multiple copies of the deterministic model in (2) but with random parameters to study population-level behavior.

III. RESULTS

Here, we reveal how the interplay between self-activation and scarcity of shared resources shapes the stability profile of (2), its robustness to noise, and the population-level distribution of these properties accounting for cellular heterogeneity.

A. Stability Analysis: Self-Activation Counteracts Loading

In the absence of self-activation ($s = 0$), the system in (2) is bistable if $q_0 < 1$ with $q_0 = 2(1 + \beta)/\alpha$, and monostable if $q_0 > 1$ [21]. Here, we reveal how positive feedback via self-activation shapes the above result.

Proposition 1. *For $0 < s \leq 1$ introduce*

$$q = \frac{2[1 + \beta(1 + s)]}{\alpha(1 + s)}, \qquad r = \frac{\beta}{a\alpha - b}, \qquad (3)$$

$$a = \frac{\sqrt{s}}{2}, \qquad b = \frac{1 + s}{4s}. \qquad (4)$$

The system in (2) *is monostable if $q > 1$, bistable if $q < 1$ and $r \notin [0, 1]$, and tristable if $0 < r < 1$.*

Proof. The proof consists of three main steps: revealing that potential fixed points belong to three manifolds; determining the number of equilibria in each case based on q and r; and concluding mono/bi/tristability combining the first two steps.

Step 1: As (y, z) must satisfy $sy^2z^3 - (y + sy + sy^3)z^2 + (1 + y^2 + sy^2)z - y = 0$ at the equilibrium of (2), we obtain that $y = z$ or $yz = 1$ or $syz = 1$, defining three manifolds.

Step 2: Next, we determine the number of positive fixed points of (2) for each of the manifolds uncovered in Step 1.

Manifold #1: Substituting $y = z$ into (2) yields

$$\frac{\alpha(1 + sz^2)}{(1 + z^2) + 2\beta(1 + sz^2)} = z \qquad (5)$$

at an equilibrium. While the right hand side of (5) increases with z, the left hand side decreases, hence there is a unique positive fixed point when $y = z$.

Manifold #2: Substituting $y = 1/z$ into (2) yields $z^2 - 2z/q + 1 = 0$ at an equilibrium. Therefore, there are two real (positive) solutions if $q < 1$, otherwise there are none.

Manifold #3: Substituting $y = 1/(sz)$ into (2) yields

$$p_1 z^4 + p_2 z^3 + p_3 z^2 + p_4 z + p_5 = 0 \qquad (6)$$

with $p_1 = s^2(1 + \beta + s\beta)$, $p_2 = -\alpha s^2(1 + s)$, $p_3 = 1 + s^2 + 2s\beta(1 + s)$, $p_4 = -\alpha s(1 + s)$, $p_5 = 1 + \beta(1 + s)$ at an equilibrium. Therefore, (6) has two positive roots if its discriminant is negative, otherwise it has no positive roots [30], where the discriminant is $\Delta_4 = \Delta_{4,1}\Delta_{4,2}^2$ with

$$\Delta_{4,1} = (1 + s)^2 - 4s\left(\alpha^2 s^2 - 4\beta^2 s - 2\beta s - 2\beta\right),$$
$$\Delta_{4,2} = s(1 + s)\left(8s - 4\beta + 4\beta s + 4\beta s^2 - 4\beta s^3\right.$$
$$\left. - 4s^2 + \alpha^2 s^2 + 2\alpha^2 s^3 + \alpha^2 s^4 - 4\right).$$

As $\Delta_{4,1} = 4s^3[(b + \beta^2)/a^2 - \alpha^2]$ with a and b from (4), (6) has two positive roots if $\beta < a\alpha - b$, otherwise it has none. Note that $a\alpha - b < 0$ leads to the latter case as $b \geq 0$, and conversely, the condition $a\alpha - b > 0$ together with $\beta < a\alpha - b$ can be captured via $0 < r < 1$ from (3).

Step 3: In summary, manifold #1 ($y = z$) yields one positive solution, maifold #2 ($yz = 1$) yields two if $q < 1$ and zero if $q > 1$, whereas manifold #3 ($syz = 1$) leads to two positive roots if $0 < r < 1$ and to zero otherwise. Therefore, the only thing left to show is that $0 < r < 1$ implies $q < 1$ to conclude the proof.
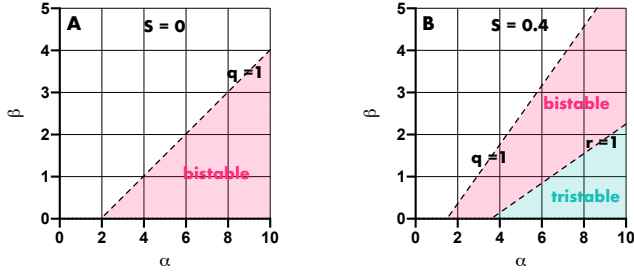
Fig. 2. Self-activation shapes the stability profile of (2) via q and r from (3): the system is monostable if $q > 1$ (unshaded region), bistable if $q < 1$ and $r \notin [0, 1]$ (red shaded region), and tristable if $0 < r < 1$ (green shaded region).

To this end, note that $q = 1$ and $r = 1$ yield $\beta = \alpha/2 - 1/(1+s)$ and $\beta = a\alpha - b$, respectively, two linear constraints in the (α, β) space (Fig. 2B). The corresponding two intercepts with the α-axis ($\beta = 0$) are given by $\alpha_1 = 1/s$ and $\alpha_2 = b/a$, respectively, and it can be verified numerically that $\alpha_1 < \alpha_2$ for $0 < s < 1$, so that the $q = 1$ constraint has an intercept with the α-axis to the left from that of the $r = 1$ constraint (Fig. 2B). Furthermore, the slope of the $q = 1$ and $r = 1$ constraints are $1/2$ and $\sqrt{s}/2$, respectively, hence the $r = 1$ constraint not only starts to the right from the $q = 1$ constraint, but it also increases slower. Therefore, the $r = 1$ line remains below the $q = 1$ line for $0 < s < 1$, thus $0 < r < 1$ indeed implies $q < 1$ (Fig. 2B). Finally, stability of the fixed points can be determined using nullcline analysis or via linearization, see [21] for more details. $\square$

In the absence of positive feedback via self-activation (e.g., $s = 0$), the system is bistable if $q < 1$ and monostable otherwise (Fig. 2A). Increasing s causes not only the $q = 1$ constraint to shift upwards, thus decreasing the region of monostability, but it pushes the $r = 1$ constraint upwards as well, giving rise to tristable dynamics (Fig. 2B). Therefore, while resource competition pushes (2) towards monostability by increasing q in (3), self-activation s counterbalances this by decreasing q, thus driving the dynamics towards multistability. In particular, once the dynamics become multistable ($q < 1$), the value of r in (3) determines whether the system displays bistable or tristable behavior.

B. Robustness Analysis: Self-Activation can be Detrimental

Rewrite (2) with $x = (y, z)$ as $\dot{y} = f(x)$ and $\dot{z} = g(x)$, and introduce the overdamped Langevin dynamics

$$\dot{y} = f(x) + \sqrt{2\epsilon}\xi_1, \qquad \dot{z} = g(x) + \sqrt{2\epsilon}\xi_2, \qquad (7)$$

where $\xi = (\xi_1, \xi_2)$ is zero-mean δ-correlated Gaussian white noise, with ϵ regulating its intensity in (7) [26], [27], [28], [29]. Due to this noise, trajectories occasionally leave the stable fixed points uncovered in Section III.A, rendering them metastable [26], [27], [28], [29].

To study their robustness to noise, we consider the average time trajectories spend near one before transitioning towards another. From [28], [29], this can be quantified by $\tau_{x_i}^{x_j} = \inf\{t > 0 : x \in \Omega_j\}$ and $\tau_{x_i}^{\{x_j, x_k\}} = \inf\{t > 0 : x \in \Omega_j \cup \Omega_k\}$,

where x_i, x_j, and x_k are stable fixed points of (2), x denotes the trajectory of (7) such that $x(0) = x_i$ and $\Omega_j \in \mathbb{R}^2$ is the basin of attraction of x_j considering (2). To efficiently compute these times, exit events from the metastable regions are often approximated by a Markov jump process [31], where the transition rates are parametrized using the Eyring–Kramers formula [26], [27], [28], [29]. To follow this strategy, we first need to define a potential landscape for (2).

Since $\partial f/\partial z \neq \partial g/\partial y$, the dynamics in (2) do not correspond to a gradient system, hence we need to define a quasi-potential $V_q(\cdot)$ that behaves as a Lyapunov function [32], [33]. That is, trajectories flow downhill on the quasi-potential surface as $\Delta V_q < 0$, reaching its local minima at stable fixed points ($\Delta V_q = 0$). The two most common choices for such quasi-potentials are introduced in [32] and [33]. In this manuscript we consider the former one, thus all experiments are carried out following the steps outlined in [32] with the quasi-potential numerically computed as

$$\Delta V_q(x) = -\left[f^2(x) + g^2(x)\right]\Delta t \qquad (8)$$

for a sufficiently small time step Δt [32], [34].

The potential barrier to reach x_j from x_i is defined as

$$H(x_i, x_j) = \inf_{\gamma:\, x_i \to x_j}\ \sup_{x^* \in \gamma} V(x^*) - V(x_i),$$

considering all continuous paths γ leading from x_i to x_j [26]. In the bistable case introduce $h_b = H(x_1, x_2) = H(x_2, x_1)$, whereas in the tristable case define $h_b = \min_{x \in \{x_2, x_3\}} H(x_1, x) = \min_{x \in \{x_1, x_3\}} H(x_2, x)$ and $h_t = H(x_3, x_1) = H(x_3, x_2)$. Therefore, h_b and h_t capture the potential barriers to leave the red/green and purple fixed points in Fig. 1B, respectively. According to the Eyring-Kramers formula, in the bistable case $\tau_{x_1}^{x_2} = \tau_{x_2}^{x_1} \propto \exp(h_b)$ as $\epsilon \to 0$, together with $\tau_{x_1}^{\{x_2, x_3\}} = \tau_{x_2}^{\{x_1, x_3\}} \propto \exp(h_b)$ and $\tau_{x_3}^{\{x_1, x_2\}} \propto \exp(h_t)$ in the tristable case (for more details, see Remark 3.4 and Example 3.5 in [26]). In the absence of self-activation ($s = 0$), stochastic numerical simulations show great agreement with predictions using the above approach [35], thus validating the use of $V_q(\cdot)$ defined in (8) for studying the robustness of (2) to noise considering (7). Thus, we next reveal how self-activation via s shapes the potential barriers h_b and h_t, hence the robustness of the fixed points in Fig. 1B to noise.

According to Prop. 1, self-activation pushes the dynamics towards multistability by decreasing q (Fig. 3A). While weak self-activation in the bistable region can slightly increase h_b (Fig. 3B, non-shaded), this effect quickly diminishes by further increasing s, and crossing into the tristable region the middle fixed point (purple in Fig. 1B) becomes dominant (Fig. 3B, shaded), effectively rendering the toggle switch to behave as if it was monostable. This effect is especially pronounced for low values of β.

To better understand this, note that in the absence of self-activation ($s = 0$), h_b can be well-approximated by the expression $h_b \approx h_{b,1}(1/q - 1)^{h_{b,2}}$ for a suitable choice of $h_{b,1}$ and $h_{b,2}$ [35]. This expression is not surprising as the distance of q from its critical value of one measures how far the dynamics lie from the mono/bistable border (Fig. 2). Remarkably, the above
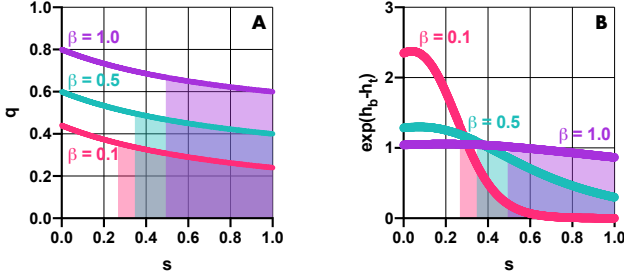
Fig. 3. While self-activation s pushes the dynamics towards tristability (Prop. 1), high values of s can render (7) to behave as if it was monostable. (A) Increasing s decreases q according to (3). (B) Increasing s can render the middle stable fixed point (purple in Fig. 1B) far more robust to noise at the expense of the other two stable equilibria (red and green in Fig. 1B). Shaded/unshaded regions denote tri/bistability, respectively ($\alpha = 5$).

Fig. 4. The potential barrier h_t to leave the middle stable fixed point in the tristable case (purple in Fig. 1B) shows (A) weak connection with r, but (B) extremely strong dependence on q. Numerical simulations correspond to samples of the typical parameter range $2 \leq \alpha \leq 10$, $0 \leq \beta \leq 2$ [21].

relationship between h_b and q provides a good approximation even when $s > 0$, however, $h_{b,1}$ and $h_{b,2}$ in this case depend on the value of s: e.g., $(h_{b,1}, h_{b,2}) = (0.56, 2.02)$ for $s = 0$ and $(h_{b,1}, h_{b,2}) = (0.49, 1.92)$ for $s = 0.3$ (with $R^2 > 0.99$).

While r from (3) establishes the bi/tristable transition (Prop. 1), h_t shows only minor dependence on this critical variable (Fig. 4A). Instead, h_t depends strongly on q (Fig. 4B) as $h_t \approx h_{t,1}(1/q - 1)^{h_{t,2}}$, where $h_{t,1}$ and $h_{t,2}$ are a function of s: e.g., $(h_{t,1}, h_{t,2}) = (0.21, 2.71)$ for $s = 0.25$ and $(h_{t,1}, h_{t,2}) = (0.15, 2.89)$ for $s = 0.50$ (with $R^2 > 0.99$). As lower β amplifies the effect of s on lowering q according to (3), the effects on both h_b and h_t are amplified, yielding more drastic changes as self-activation increases (Fig. 3B). By rendering the middle fixed point (purple in Fig. 1B) dominant over the "bistable" ones (red and green in Fig. 1B), the system thus approaches a behavior that resembles monostability (despite the underlying tristable dynamics) in the case of strong self-activation.

C. Population-Level Analysis for Cellular Heterogeneity

To account for the variability ubiquitous to cells, we next consider the case when α and β are random variables. In particular, assume that $X = (\alpha, \beta) \sim \mathcal{N}(\mu, \Sigma)$ with

$$\mu = \begin{pmatrix} \mu_\alpha \\ \mu_\beta \end{pmatrix}, \qquad \Sigma = \begin{bmatrix} \sigma_\alpha^2 & \rho\sigma_\alpha\sigma_\beta \\ \rho\sigma_\beta\sigma_\alpha & \sigma_\beta^2 \end{bmatrix}. \quad (9)$$

Based on the analysis in Sections III.A and III.B, it follows that the population-level stability and robustness profiles depend on the random variables

$$Q = \frac{2[1 + \beta(1+s)]}{\alpha(1+s)}, \qquad R = \frac{\beta}{a\alpha - b}. \quad (10)$$

In particular, the probability that (2) yields monostable dynamics is $p_{\text{mono}} = \mathbf{P}(Q > 1)$, whereas the probability of tristability and bistability are given by $p_{\text{tri}} = \mathbf{P}(0 < R < 1)$ and $p_{\text{bi}} = 1 - p_{\text{mono}} - p_{\text{tri}}$, respectively. To reveal what role loading and self-activation play in establishing population-level characteristics, we next introduce an approximation of the distributions of Q and R using the following Lemma, adopted from [22], reformulating the results in [36], [37].

Lemma 1. *Let $X \in \mathbb{R}^N$ be a jointly normal random variable with mean vector $\mu \in \mathbb{R}^N$ and covariance matrix $\Sigma \in \mathbb{R}^{N \times N}$.*
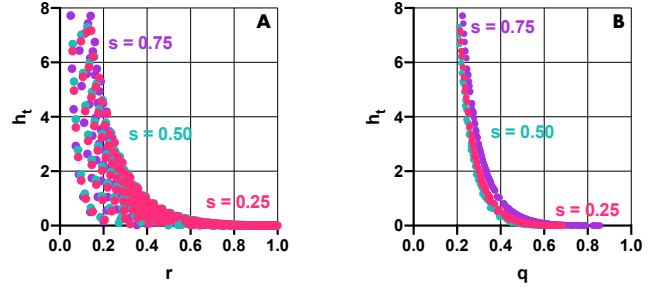
Introduce $A, C \in \mathbb{R}^N$, $B, D \in \mathbb{R}$, the random variable $W = (A^\top X + B)/(C^\top X + D)$ together with

$$F(w) = \Phi\left(\frac{w - \mu_W}{\sigma_W(w)}\right), \quad (11)$$

where $\Phi(\cdot)$ is the cdf of the standard normal distribution and $\mu_W = (B + A^\top \mu)/(D + C^\top \mu)$, $\sigma_W(w) = \sqrt{(A - Cw)^\top \Sigma (A - Cw)}/(D + C^\top \mu)$. With this, $|\mathbf{P}(W < w) - F(w)| \leq \Phi\left(-\frac{C^\top \mu + D}{\sqrt{C^\top \Sigma C}}\right)$.

Therefore, with the notation of Lemma 1, for Q in (10) we have $A^\top = [0 \ \ 2 + 2s]$, $B = 2$, $C^\top = [1 + s \ \ 0]$, and $D = 0$, whereas for R we have $A^\top = [0 \ \ 1]$, $B = 0$, $C^\top = [a \ \ 0]$, and $D = -b$. Thus, with $\mu_Q = 2[1 + \mu_\beta(1+s)]/[\mu_\alpha(1+s)]$, $\mu_R = \mu_\beta/(a\mu_\alpha - b)$, and

$$\begin{aligned} \sigma_Q(q) &= \frac{\sqrt{4\sigma_\beta^2 + q^2\sigma_\alpha^2 - 4\rho q \sigma_\alpha \sigma_\beta}}{\mu_\alpha}, \\ \sigma_R(r) &= \frac{\sqrt{\sigma_\beta^2 + \sigma_\alpha^2 r^2 a^2 - 2\rho r \sigma_\alpha \sigma_\beta a}}{a\mu_\alpha - b}, \end{aligned} \quad (12)$$

we obtain the approximate distribution of both Q and R as

$$\mathbf{P}(Q < q) = \Phi\left(\frac{q - \mu_Q}{\sigma_Q(q)}\right), \quad \mathbf{P}(R < r) = \Phi\left(\frac{r - \mu_R}{\sigma_R(r)}\right),$$

thus revealing how self-activation and competition for shared cellular resources affect the population-level stability and robustness properties of (2).

We first obtain that the probability of monostability, or alternatively, the unimodal fraction of the population is

$$p_{\text{mono}} = 1 - \Phi\left(\frac{1 - \mu_Q}{\sigma_Q(1)}\right) = \Phi\left(\frac{\mu_Q - 1}{\sigma_Q(1)}\right), \quad (13)$$

and the multimodal fraction is expected to be $1 - p_{\text{mono}}$. This reveals not only how self-activation shifts the population towards multimodality (Fig. 5A), but also that uniformity increases with the correlation ρ between α and β by decreasing $\sigma_Q(q)$ according to (12). Thus, increasing ρ from -1 to +1 decreases the unimodal fraction of the population from 15% to less than 0.5% (Fig. 5B). Further dividing the multimodal
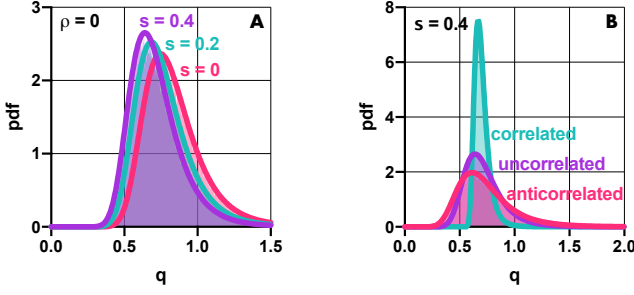
Fig. 5. Self activation s shapes the population-level behavior via Q and R. (A) Self-activation affects μ_Q but not σ_Q, (B) correlation ρ the other way around. Solid lines and shaded regions denote the approximations from Section III.B and the pdf obtained by numerical simulations, respectively. Simulation parameters are $\mu_\alpha = 5$, $\mu_\beta = 1$, $\sigma_\alpha = \mu_\alpha/5$, $\sigma_\beta = \mu_\beta/5$.
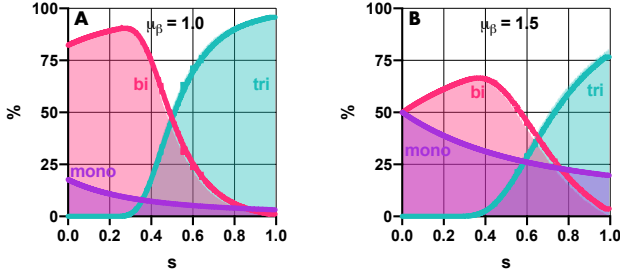

Fig. 6. Self-activation promotes the emergence of multimodal populations. Solid lines and shaded regions denote the approximations in (13)–(14) and the pdf obtained by numerical simulations, respectively. Simulation parameters are $\mu_\alpha = 5$, $\sigma_\alpha = \mu_\alpha/5$, $\sigma_\beta = \mu_\beta/5$, and $\rho = 0$.

portion of the population, the trimodal and bimodal fractions are given by $p_{\text{tri}} = \mathbf{P}(0 < R < 1)$ and $p_{\text{bi}} = 1 - p_{\text{mono}} - p_{\text{tri}}$:

$$p_{\text{tri}} = \Phi\left(\frac{1 - \mu_R}{\sigma_R(1)}\right) + \Phi\left(\frac{\mu_\beta}{\sigma_\beta}\right) - 1,$$
$$p_{\text{bi}} = \Phi\left(\frac{\mu_Q - 1}{\sigma_Q(1)}\right) + \Phi\left(\frac{1 - \mu_R}{\sigma_R(1)}\right) + \Phi\left(\frac{\mu_\beta}{\sigma_\beta}\right), \quad (14)$$

confirmed in Fig. 6. While self-activation first increases the bimodal fraction of the population, it is quickly replaced with trimodality by further increasing s. Finally, to obtain the population-level distribution of robustness properties, it is sufficient to find the distribution of the potential barriers h_b and h_t, which are simple transformations of the probability distribution of Q as $h_b \approx h_{b,1}(1/q - 1)^{h_{b,2}}$ and $h_t \approx h_{t,1}(1/q - 1)^{h_{t,2}}$ from Section III.B.

IV. APPLICATION EXAMPLE

Here, we reveal how their context affects the stability and robustness properties of genetic switches, and how self-activation shapes this effect. Due to competition for shared resources originating in the genetic context of y and z, the dynamics in (2) change according to

$$\dot{y} = \frac{\frac{\alpha}{1+z^2} + \frac{s\alpha y^2}{1+y^2}}{1 + \frac{\beta}{1+y^2} + \frac{\beta}{1+z^2} + \frac{s\beta y^2}{1+y^2} + \frac{s\beta z^2}{1+z^2} + \beta_c} - y,$$
$$\dot{z} = \frac{\frac{\alpha}{1+y^2} + \frac{s\alpha z^2}{1+z^2}}{1 + \frac{\beta}{1+y^2} + \frac{\beta}{1+z^2} + \frac{s\beta y^2}{1+y^2} + \frac{s\beta z^2}{1+z^2} + \beta_c} - z, \quad (15)$$
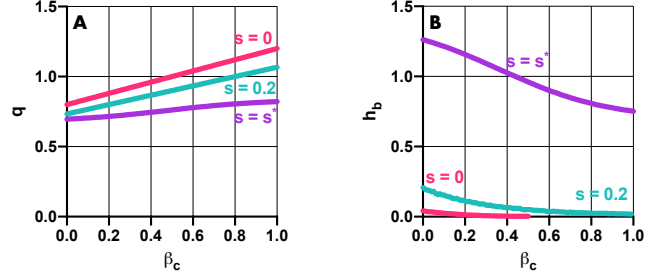

Fig. 7. The context of the toggle switch affects its stability and robustness properties (A) by pushing it towards monostability and (B) by decreasing the potential barrier h_b. These effects can be mitigated by stronger self-activation via increasing s, for instance, to the value s^* such that $r = 1$. Simulation parameters: $\alpha = 5$, $\beta = 1$.

where β_c can be interpreted similarly to β, capturing the loading effects due to expressing proteins other than y and z [21]. As the rescalings $\alpha \leftarrow \alpha/(1+\beta_c)$ and $\beta \leftarrow \beta/(1+\beta_c)$ render the dynamics (15) to become (2), the results derived in this paper apply to even in the presence of additional loading from the context of the toggle switch. For instance, the expression of q from (3) now yields

$$q = \frac{2[1 + \beta(1+s)]}{\alpha(1+s)} \frac{1 + \beta(1+s) + \beta_c}{1 + \beta(1+s)}. \quad (16)$$

Therefore, by increasing q, β_c pushes the toggle switch towards both monostability (Fig. 7A) and decreased robustness to noise (Fig. 7B). This effect, however, can be mitigated by s: from (16) it also follows that increasing s decreases the effects of β_c on q (Fig. 7A). Furthermore, stronger self-activation s not only provides increased robustness to noise by raising the potential barrier h_b (Fig. 7B), but it also extends the critical value of β_c eventually pushing the toggle switch into the monostable regime ($q > 1$).

Therefore, it would be tempting to conclude that to minimize perturbations from the context, one should increase the value of s until $r = 1$, thus the toggle switch is on the border of bi/tristability (Prop. 1). While this indeed reduces the effect of the context on the toggle switch, e.g., the decrease in h_b (Fig. 7B), it comes at a price, as both the robustness of the middle fixed point and the trimodal fraction of the population can increase significantly (Fig. 3 and Fig. 6).

V. CONCLUSION

Multistable switches are fundamental in both natural and engineered systems, thus understanding how their behavior is shaped by context-dependence is crucial for systems and synthetic biology. As scarcity of shared resources presents a major source of context-dependence, here we focused on the interplay between competition for these resources and self-activation, a prominent feature of multistable genetic switches.

Our results reveal that while competition pushes the dynamics towards monostability, self-activation attenuates this adverse effect. As self-activation also mitigates the effect of loading from the context of the switch, strong self-activation might seem preferable. While weak self-activation indeed increases robustness to both noise and external perturbations due to loading from the context, strong self-activation can render

the tristable system appear as if it was monostable (Fig. 3), which can be especially troubling when tuning biophysical parameters. To illustrate this, consider the case when three different steady states are observed with a dominant middle fixed point. One could conclude that the population is a mixture of monostable and bistable cells (e.g., $s = 0.2$ in Fig. 6), thus self-activation should be increased to eliminate the unimodal subpopulation. Alternatively, the above behavior can also be a result of the mixture of bistable and tristable cells (e.g., $s = 0.8$ in Fig. 6), in which case self-activation must be decreased to eliminate the trimodal subpopulation.

By revealing the role that s plays in establishing stability and robustness properties both at single cell and population levels, we expect our results to guide the data-driven design of multistable genetic switches, especially as s can be tuned with external inputs [38]. Future research will focus on the experimental verification of these findings, and on the deeper analysis of the relationship between robustness to noise and the value of q and r, even in the case of alternative quasi-potentials [33]. Finally, while the overdamped approximation of the Langevin dynamics is valid where the particle inertia is negligible compared to the damping force [39], we seek to explore the performance and applicability of the proposed method for the standard Langevin dynamics instead of the overdamped approximation considered in this manuscript.

REFERENCES

[1] Y. Qian, C. McBride, and D. Del Vecchio, "Programming cells to work for us," *Annual Review of Control, Robotics, and Autonomous Systems*, vol. 1, no. 1, pp. 411–440, 2018.

[2] S. Cardinale and A. P. Arkin, "Contextualizing context for synthetic biology–identifying causes of failure of synthetic biological systems." *Biotechnology Journal*, vol. 7, no. 7, pp. 856–866, 2012.

[3] E. Yeung, A. J. Dy, K. B. Martin, A. H. Ng, D. Del Vecchio, J. L. Beck, J. J. Collins, and R. M. Murray, "Biophysical Constraints Arising from Compositional Context in Synthetic Gene Networks." *Cell systems*, vol. 5, no. 1, pp. 11–24.e12, July 2017.

[4] L. B. Andrews, A. A. K. Nielsen, and C. A. Voigt, "Cellular checkpoint control using programmable sequential logic," *Science*, vol. 361, no. 6408, p. eaap8987, Sept. 2018.

[5] J. A. J. Arpino, E. J. Hancock, J. Anderson, M. Barahona, G.-B. V. Stan, A. Papachristodoulou, and K. Polizzi, "Tuning the dials of Synthetic Biology," *Microbiol*, vol. 159, no. 7, pp. 1236–1253, 2013.

[6] A. Y. Weiße, D. A. Oyarzún, V. Danos, and P. S. Swain, "Mechanistic links between cellular trade-offs, gene expression, and growth," *PNAS*, vol. 112, no. 9, pp. E1038–E1047, 2015.

[7] D. Siegal-Gaskins, Z. A. Tuza, J. Kim, V. Noireaux, and R. M. Murray, "Gene Circuit Performance Characterization and Resource Usage in a Cell-Free "Breadboard"," *ACS Synth Biol*, vol. 3, pp. 416–425, 2014.

[8] F. Ceroni, R. Algar, G.-B. Stan, and T. Ellis, "Quantifying cellular capacity identifies gene expression designs with reduced burden." *Nature Methods*, vol. 12, no. 5, pp. 415–418, 2015.

[9] A. Gyorgy, J. I. Jiménez, J. Yazbek, H.-H. Huang, H. Chung, R. Weiss, and D. Del Vecchio, "Isocost Lines Describe the Cellular Economy of Genetic Circuits," *Biophys J*, vol. 109, no. 3, pp. 639–646, 2015.

[10] A. Raveh, M. Margaliot, E. D. Sontag, and T. Tuller, "A model for competition for ribosomes in the cell." *Journal of The Royal Society Interface*, vol. 13, no. 116, Mar. 2016.

[11] Y. Qian, H.-H. Huang, J. I. Jiménez, and D. Del Vecchio, "Resource Competition Shapes the Response of Genetic Circuits," *ACS Synthetic Biology*, vol. 6, no. 7, pp. 1263–1272, 2017.

[12] D. D. Vecchio, Y. Qian, R. M. Murray, and E. D. Sontag, "Future systems and control research in synthetic biology," *Annual Reviews in Control*, vol. 45, pp. 5 – 17, 2018.

[13] L. Bandiera, Z. Hou, V. B. Kothamachu, E. Balsa-Canto, P. S. Swain, and F. Menolascina, "On-line optimal input design increases the efficiency and accuracy of the modelling of an inducible synthetic promoter," *Processes*, vol. 6, no. 9, 2018.

[14] M. Chaves and D. A. Oyarzún, "Dynamics of complex feedback architectures in metabolic pathways," *Automatica*, vol. 99, pp. 323–332, 2019.

[15] A. Gyorgy and R. M. Murray, "Quantifying resource competition and its effects in the TX-TL system," in *55th IEEE Conference on Decision and Control (CDC)*. IEEE, 2016, pp. 3363–3368.

[16] T. S. Gardner, C. R. Cantor, and J. J. Collins, "Construction of a genetic toggle switch in E. coli," *Nature*, vol. 403, pp. 339–42, 2000.

[17] E. M. Ozbudak, M. Thattai, H. N. Lim, B. I. Shraiman, and A. van Oudenaarden, "Multistability in the lactose utilization network of Escherichia coli," *Nature*, vol. 427, no. 6976, pp. 737–740, 2004.

[18] R. Guantes and J. F. Poyatos, "Multistable decision switches for flexible control of epigenetic differentiation," *PLOS Computational Biology*, vol. 4, no. 11, pp. 1–13, 11 2008.

[19] O. Purcell, M. di Bernardo, C. S. Grierson, and N. J. Savery, "A multi-functional synthetic gene network: A frequency multiplier, oscillator and switch," *PLOS ONE*, vol. 6, no. 2, pp. 1–12, 2011.

[20] C. Cuba Samaniego and E. Franco, "A robust molecular network motif for period-doubling devices," *ACS Synthetic Biology*, vol. 7, no. 1, pp. 75–85, 2018, pMID: 29227103.

[21] A. Gyoryg, "Sharing resources can lead to monostability in a network of bistable toggle switches," *IEEE Control Systems Letters*, vol. 3, no. 2, pp. 308–313, 2018.

[22] A. Gyorgy, "How Cell-to-Cell Heterogeneity and Scarce Resources Shape the Population-Level Stability Profile of Toggle Switches," in *58th IEEE Conference on Decision and Control (CDC)*, 2019, p. k.

[23] A. E. Blanchard, C. Liao, and T. Lu, "Circuit-host coupling induces multifaceted behavioral modulations of a gene switch," *Biophysical Journal*, vol. 114, no. 3, pp. 737 – 746, 2018.

[24] M. Leon, M. L. Woods, A. J. H. Fedorec, and C. P. Barnes, "A computational method for the investigation of multistable systems and its application to genetic switches," *BMC Systems Biology*, vol. 10, no. 1, p. 130, 2016.

[25] A. Gyorgy, "Bistability requires better balanced toggle switches in the presence of competition for shared cellular resources," in *American Control Conference (ACC)*, 2019, pp. 154–1546.

[26] N. Berglund, "Kramers' law: Validity, derivations and generalisations," *Markov Processes and Related Fields*, vol. 19, pp. 459–490, 2013.

[27] F. Bouchet and J. Reygner, "Generalisation of the Eyring–Kramers transition rate formula to irreversible diffusion processes," *Annales Henri Poincaré*, vol. 17, pp. 3499–3532, 2016.

[28] T. Lelièvre, D. Le Peutrec, and B. Nectoux, "Exit event from a metastable state and Eyring-Kramers law for the overdamped Langevin dynamics," in *Stochastic Dynamics Out of Equilibrium*, G. Giacomin, S. Olla, E. Saada, H. Spohn, and G. Stoltz, Eds. Cham: Springer International Publishing, 2019, pp. 331–363.

[29] G. D. Gesu, T. Lelievre, D. L. Peutrec, and B. Nectoux, "Sharp asymptotics of the first exit point density," *Annals of PDE*, vol. 5, no. 1, p. 5, Mar 2019.

[30] W. Beyer, *CRC handbook of mathematical sciences*. CRC Press, 1987.

[31] M. R. So/rensen and A. F. Voter, "Temperature-accelerated dynamics for simulation of infrequent events," *The Journal of Chemical Physics*, vol. 112, no. 21, pp. 9599–9606, 2000.

[32] S. Bhattacharya, Q. Zhang, and M. E. Andersen, "A deterministic map of Waddington's epigenetic landscape for cell fate specification," *BMC Systems Biology*, vol. 5, no. 1, p. 85, Dec. 2011.

[33] K.-Y. Kim and J. Wang, "Potential energy landscape and robustness of a gene regulatory network: Toggle switch," *PLOS Computational Biology*, vol. 3, no. 3, pp. 1–13, 03 2007.

[34] B. Verd, A. Crombach, and J. Jaeger, "Classification of transient behaviours in a time-dependent toggle switch model," *BMC Systems Biology*, vol. 8, no. 1, p. 43, Apr 2014.

[35] A. Gyorgy, "Scarcity of Cellular Resources Decreases the Robustness of Toggle Switches to Noise," in *American Control Conference (ACC)*, 2020 (Accepted).

[36] D.V. Hinkley, "On the Ratio of Two Correlated Normal Random Variables," *Biometrika*, vol. 56 (3), no. 3, pp. 635–639, 1969.

[37] R. C. Geary, "The Frequency Distribution of the Quotient of Two Normal Variates, Tech. Rep. 3, 1930.

[38] T. Li, Y. Dong, X. Zhang, X. Ji, C. Luo, C. Lou, H. M. Zhang, and Q. Ouyang, "Engineering of a genetic circuit with regulatable multistability," *Integr Biol*, vol. 10, no. 8, pp. 474–482, 07 2018.

[39] R. Pan, T. M. Hoang, Z. Fei, T. Qiu, J. Ahn, T. Li, and H. T. Quan, "Quantifying the validity and breakdown of the overdamped approximation in stochastic thermodynamics: Theory and experiment," *Phys. Rev. E*, vol. 98, p. 052105, Nov 2018.